Ge/SiGe quantum wells on Si(111): Growth, structural, and optical properties

E. Gatti, F. Isa, D. Chrastina, E. Müller Gubler, F. Pezzoli, E. Grilli, and G. Isella

Citation: Journal of Applied Physics **116**, 043518 (2014); doi: 10.1063/1.4891463
View online: http://dx.doi.org/10.1063/1.4891463
View Table of Contents: http://scitation.aip.org/content/aip/journal/jap/116/4?ver=pdfcov
Published by the AIP Publishing

Ge/SiGe quantum wells on Si(111): Growth, structural, and optical properties

E. Gatti,[1,a)] F. Isa,[2] D. Chrastina,[2] E. Müller Gubler,[3] F. Pezzoli,[1] E. Grilli,[1] and G. Isella[2]
[1]*L-NESS and Dipartimento di Scienza dei Materiali, Università di Milano Bicocca, via Cozzi 55, I-20125 Milano, Italy*
[2]*L-NESS and Dipartimento di Fisica, Politecnico di Milano, Polo di Como, via Anzani 42, I - 22100 Como, Italy*
[3]*Electron Microscopy Center of ETH Zürich (EMEZ), August-Piccard-Hof 1, CH-8093 Zürich, Switzerland*

(Received 17 April 2014; accepted 15 July 2014; published online 29 July 2014)

The epitaxial growth of $Ge/Si_{0.15}Ge_{0.85}$ multiple quantum wells (MQWs) on Si(111) substrates is demonstrated. A 3 μm thick *reverse, double-step* virtual substrate with a final composition of $Si_{0.10}Ge_{0.90}$ has been employed. High resolution XRD, TEM, AFM and defect etching analysis has been used for the study of the structural properties of the buffer and of the QWs. The QW stack is characterized by a threading dislocation density of about $3 \times 10^7\,cm^{-2}$ and an interdiffusion layer at the well/barrier interface of 2.1 nm. The quantum confined energy levels of this system have been calculated using the k·p and effective mass approximation methods. The $Ge/Si_{0.15}Ge_{0.85}$ MQWs have been characterized through absorption and photoluminescence measurements. The optical spectra have been compared with those of $Ge/Si_{0.15}Ge_{0.85}$ QWs grown on Si(001) through a thick graded virtual substrate. © *2014 AIP Publishing LLC*. [http://dx.doi.org/10.1063/1.4891463]

I. INTRODUCTION

In recent years, different approaches have been proposed to satisfy the challenging request of integration of optical functionalities on the Si-based CMOS platform. Ge-based systems are interesting for this purpose, due to Ge and SiGe alloy integrability on Si and to the pseudo-direct nature of Ge band structure, which is characterized by a direct band gap in the spectral region of the C band used in telecommunication. Ge/SiGe multiple quantum wells (MQWs) have been demonstrated to be one of the most promising Ge-rich structures, thanks to the type-I band alignment and to the possibility of tailoring the optical transition energies with strain and composition. Indeed, their optical,[1–5] structural,[4] and spin properties[6] have been widely studied. Furthermore, low-loss photonic interconnects,[7] optical spin tailoring,[8] and room temperature (RT) electroluminescence[9,10] have all been demonstrated in Ge MQWs. Moreover, the application of these heterostructures for thermoelectric energy generation has also been recently investigated.[11]

Most of the literature works on this topic are focused on Ge/SiGe QWs grown on Si(001), which is the surface orientation commonly used in CMOS technology. The integration of Ge-rich epitaxial layers on Si(001) can be achieved using graded virtual substrates (GVSs), in which the Ge content linearly varies from zero to the desired final composition (see, e.g., Refs. 12 and 13). This approach provides a moderate threading dislocation density (TDD) of about $10^6\,cm^{-2}$.[14] GVSs with a composition grading of 7% per μm and thus with a typical thickness of 12–15 μm have been employed for the growth of Ge/SiGe QWs on Si(001).[2] The high optical quality of these QWs is demonstrated by the presence of sharp excitonic peaks in RT absorption (ABS) spectra[2] and by the observation of direct and indirect emission in RT photoluminescence (PL) spectra.[15] The use of GVSs limits the application of these systems in actual devices, due to their excessive thickness and to the poor heat conduction. For these reasons, solutions employing considerably thinner virtual substrates (VSs) with composition steps or reverse grading have been proposed very recently. A critical summary of this topic can be found, e.g., in Ref. 16, where a comparison between the structural properties of different thin SiGe buffers on Si(001) is also presented. TDD values are shown to span between 5×10^6 and $8 \times 10^7\,cm^{-2}$ depending on the VS design.

The growth of high quality Ge/SiGe QWs on high index Si surfaces, such as the (111) plane, will allow the exploitation of novel properties and new potential applications of these systems. High index orientations, combined with a proper strain control, could be used for tailoring the band structure and the spin properties of Ge.[17,18] Carrier mobility can also be enhanced: Ge(111) ultrathin channels in n-MOSFETs are expected to yield higher electron mobility with respect to channels oriented along the (001) or (110) directions.[19] Moreover, dislocation dynamics strongly depends on substrate orientation. In the case of epitaxial SiGe layers under tensile strain in the (111) plane, stacking fault generation due to dislocation partialization is inhibited,[20] while it is favored during tensile strain relaxation in (001) oriented epilayers.[21] Consequently, the growth on the (111) surface may possibly be used as a further degree of freedom to improve crystal quality.

The integration of Ge QWs on Si(111) is nevertheless challenging: the conventional GVS approach cannot be used due to the difficulties in the growth of Si-rich SiGe layers on Si(111), as discussed in Refs. 22–26. Indeed, in order to obtain Ge-rich layers with a structural quality comparable to that of GVS on Si(001), a composition grading of about 1% per μm would be needed, resulting in markedly thicker GVSs.[23] Some alternative approaches for the integration of

a)Electronic mail: eleonora.gatti@mater.unimib.it

Ge-rich layers on Si(111) have been reported in the literature. The insertion of a Ge seed layer that induces an intermediate islanding step allows to obtain a surface roughness of about 2 nm, but a rather high TDD of about $3 \times 10^8\,cm^{-2}$ is still found.[25] The TDD can be reduced to values $\leq 1 \times 10^7\,cm^{-2}$ through a surfactant mediated MBE growth, but a significant impurity concentration affects the Ge layer.[27]

In this work, we propose a viable approach for the deposition of Ge-rich SiGe layers on Si(111) substrates and discuss the structural and optical properties of Ge/SiGe QWs on Si(111) grown following this approach. The proposed method for the epitaxial growth of these Ge-rich heterostructures on the Si(111) surface consists in a *reverse, double-step* virtual substrate. The structural properties of the active part of the samples are evaluated through high resolution X-ray diffraction (HR-XRD), atomic force microscopy (AFM), defect etching, and transmission electron microscopy (TEM). The quantum confined energy levels of Ge/SiGe QWs on Si(111) are calculated using the k·p method. The optical properties of the Ge/SiGe QWs are studied through ABS and PL measurements. Finally, the structural and optical properties of the Ge/SiGe QWs on Si(111) are compared with those of MQWs with the same structure grown on Si(001) through a GVS, which can be considered as a benchmark of high structural and optical quality.

II. EXPERIMENTAL

All samples have been deposited on (111) or (001) oriented Si substrates (3.5° and 0.5° miscut, respectively) by low-energy plasma-enhanced CVD (LEPECVD)[13] using silane (SiH_4) and germane (GeH_4) as precursor gases. Si wafers have been prepared using RCA cleaning. Oxide was stripped off right before insertion of the wafers in the deposition chamber, using hydrofluoridric acid.

A PANalytical X'Pert PRO MRD high resolution X-ray diffractometer equipped with a hybrid mirror and a 2-bounce asymmetric Ge monochromator was employed for HR-XRD measurements. AFM scans were obtained using a Veeco Innova microscope in tapping mode. For the TEM investigation, a dedicated scanning transmission electron microscope (Hitachi, HD2700C) equipped with a Cs-corrector (CEOS) was used in z-contrast mode (high-angle annular dark field STEM). Defect etching experiments have been performed using a Cr based solution for $Si_{0.10}Ge_{0.90}$ layers[14] and a iodine based solution for pure Ge epilayers.[28] Atomic force microscopy and Nomarski optical microscopy have been used for the etch-pit counting. The error bars on the TD density correspond to the standard deviation obtained by counting etch-pits on an area of at least $200 \times 200\,\mu m^2$ for each sample.

RT ABS measurements were performed using a Jasco V750 spectrometer equipped with a cooled PbS detector. Impinging on the sample at the Brewster angle with light linearly polarized in the incidence plane, the reflection losses and the interference effects, related to the multi-layer structure of the samples, are strongly reduced. Moreover, the ABS of the samples was corrected for that of the corresponding substrates as described in Ref. 29. In PL measurements, the 1064 nm (1.165 eV) line of a Nd:YVO_4 laser (exciting power about 440 mW, spot diameter about 50 μm) was employed for excitation; the penetration depth is about 50 QWs. The emitted light was detected by a Jasco FT-IR 800 spectrometer equipped with a PbS detector (cut-off energy at about 0.4 eV).

III. GROWTH AND STRUCTURAL PROPERTIES OF Ge/SiGe QWs on Si(111)

Due to the difficulties in the growth of GVSs on Si(111) surface, discussed in Sec. I, we have developed a *reverse, double-step* design inspired by the reverse-graded approach presented in Ref. 30. This design has been preferred to a *reverse, composition-graded* layer[30] for it allows to reduce the VS thickness.

The growth of strain-compensated Ge/SiGe QWs with Ge-rich barriers requires a VS ending with a SiGe layer whose Ge content is intermediate between the one of the wells and that of the barriers. In particular, in the case of Ge/$Si_{0.15}Ge_{0.85}$ QWs a $Si_{0.1}Ge_{0.9}$ layer is commonly adopted.[2] Ge-rich slabs directly deposited on Si are generally characterized by TDD higher than $10^8\,cm^{-2}$. While a proper *in-situ* thermal treatment of the Ge-on-Si layers can provide a reduction of the TDD of about one order of magnitude (see, e.g., Refs. 28 and 31), we have experimentally observed that the same thermal cycles applied to SiGe layers yield a significant increase of the surface roughness without a substantial reduction of TDD. Consequently, our approach implies a Ge layer deposited on Si(111) and subjected to *in-situ* annealing cycles right after the deposition. This is expected to have beneficial effects also on the layers grown on top. The required Ge-rich SiGe layer completes the VS. Additionally, at the beginning of the growth, this SiGe layer experiences a tensile strain due to the lattice constant mismatch with the Ge slab. The biaxial tensile strain at the (111) Ge/SiGe interface plane is expected to inhibit stacking fault formation and propagation towards the MQW region, as discussed in Ref. 20.

As described below, three different samples have been analyzed, which present different relaxed buffers but nominally identical MQW stacks. Their structure is schematically sketched in Fig. 1. Buffer design, substrate orientation and growth parameters are summarized in Table I.

Sample A has been grown following the above mentioned *reverse, double-step* design. It consists of a 2 μm thick Ge layer deposited on Si(111) at 500 °C with a growth rate of 4.2 nm/s. The Ge layer is then subjected *in situ* to 6 annealing cycles (600–780 °C) at a pressure of $\sim 5 \times 10^{-7}$ mbar. The Ge slab is followed by a $Si_{0.10}Ge_{0.90}$ layer, 1 μm thick, deposited at 475 °C with a growth rate of 5.0 nm/s. Finally, 50 Ge/$Si_{0.15}Ge_{0.85}$ QWs are grown at 475 °C with a growth rate of 4.2 nm/s. The nominal well and barrier thickness, designed in order to balance the compressive strain in the QWs with the tensile strain in the barriers, is 10 and 21 nm, respectively. Thus, the QW stack is pseudomorphic with respect to the relaxed $Si_{0.10}Ge_{0.90}$ layer at the top of the VS.

The structure of *sample B* is the same as the one of sample A, except for the lack of the Ge slab in the VS. The same

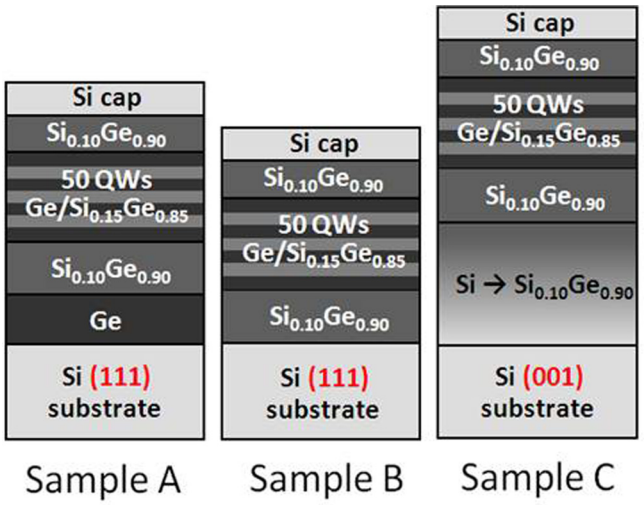

FIG. 1. Schematic of the analyzed samples.

growth parameters have been used. The sample is aimed at evidencing the effectiveness of our solution for the VS with respect to a simple SiGe layer directly grown on Si.

Finally, as a benchmark of structural and optical quality, we used an analogous $Ge/Si_{0.15}Ge_{0.85}$ MQW structure grown on Si(001) through a GVS. The GVS has been grown according to the procedure discussed in Ref. 32, and is followed by a 1 μm thick $Si_{0.10}Ge_{0.90}$ layer. In the following, we will refer to this structure as *sample C*. ABS and PL spectra of sample C have already been studied in Ref. 15.

Samples with analogous VSs but without the QW stack (named "substrates"), were also employed as references for ABS, PL, and defect etching measurements.

The structural characterization performed on sample A is summarized in Fig. 2. Panels (a) and (b) report the results of the HR-XRD analysis. Panel (a) displays the reciprocal space map around the (224) Bragg reflection. Panel (b) shows the ω-2θ scan extracted from the symmetric (333) Bragg reflection, in which the peaks at $\omega = 45.1°$ and 45.3° are related to the Ge and the $Si_{0.1}Ge_{0.9}$ layers in the buffer, respectively, and all the other periodic fringes are associated to the QW stack. The HR-XRD reciprocal space map around the (224) Bragg reflection indicates that the Ge layer in the buffer (with an actual measured Ge content of 99.8%) is under a tensile in-plane strain of 0.17%. The SiGe layer of the buffer, with a Ge content of 90.1%, is under an even higher tensile in-plane strain of 0.27%, indicating a partial degree of relaxation of the SiGe layer on Ge of about 56%. However, the superlattice satellite peaks are all aligned at the same $q_{||}$ indicating that both barriers and QWs have the same in-plane lattice parameter, $a_{||} = 0.2306 \pm 0.0001$ nm, as the VS, which indicates a good coherence of the layers in the QW stack. This can be seen clearly also in the ω-2θ scan of Fig. 2(b), where the peak related to the $Si_{0.1}Ge_{0.9}$ buffer coincides with the 0th order QW-related fringe. A period of 39.6 nm was found for Sample A. A well thickness of 12 nm is estimated.

A cross section high-angle annular dark field STEM image of the QW stack is reported in Fig. 2(c), where the Ge QW region appears brighter than the $Si_{0.15}Ge_{0.85}$ barriers. An interdiffusion region of (2.0 ± 0.5) nm at the QW/barrier interface can be estimated from our STEM data. Such a value is at the upper limit of values reported for (001) oriented Ge QWs,[4,33] which are comprised between 0.5 and 2 nm.

A defect etching analysis has been performed on substrate A, giving a TDD of $(2.7 \pm 0.6) \times 10^7\,cm^{-2}$. Thanks to strain compensation no further TDs are expected to nucleate in the QW stack.

The surface of sample A, as observed through AFM, is shown in Fig. 2(d). Surface steps are formed due to the 3.5° miscut of the (111) wafer employed for the deposition and are perpendicular to the miscut direction ([1-10] in our case). This is an indication that the growth proceeds in a step-flow regime. A RMS roughness of (2.1 ± 0.3) nm is measured on $5 \times 5\ \mu m^2$ large areas. Moreover, measurements performed on a Ge-on-Si(111) layer before the SiGe deposition indicate that at this stage the RMS roughness is already ~2 nm, therefore no additional roughening is introduced during the SiGe deposition.

The same structural analysis has also been performed on samples B and C. The values of TDD and surface roughness obtained for the different samples are summarized in

TABLE I. VS design of the analyzed samples. The growth parameters are also reported: T_{growth} and R_{growth} are the growth temperature and the growth rate, respectively. In the GVS T_{growth} and R_{growth} depend linearly on the Ge content, as described in Ref. 32.

		Buffer			
Sample	Orientation	Approach	Composition	Thickness	Growth parameters
A	(111)	Double step reverse buffer	Ge	2 μm	T_{growth}: 500 °C R_{growth}: 4.2 nm/s T_{anneal}: 600–800 °C (6 cycles)
			$Si_{0.1}Ge_{0.9}$	1 μm	T_{growth}: 475 °C R_{growth}: 5.0 nm/s
B	(111)	Constant composition layer	$Si_{0.1}Ge_{0.9}$	2 μm	T_{growth}: 475 °C R_{growth}: 5.0 nm/s
C	(001)	Graded virtual substrate	$Si \rightarrow Si_{0.1}Ge_{0.9}$ (7%/μm)	13 μm	T_{growth}: 760→520 °C R_{growth}: from Si to $Si_{0.5}Ge_{0.5}$: 4.9 → 7.4 nm/s from $Si_{0.5}Ge_{0.5}$ to $Si_{0.1}Ge_{0.9}$: 7.4 → 5.0 nm/s
			$Si_{0.1}Ge_{0.9}$	1 μm	T_{growth}: 520 °C R_{growth}: 5.0 nm/s

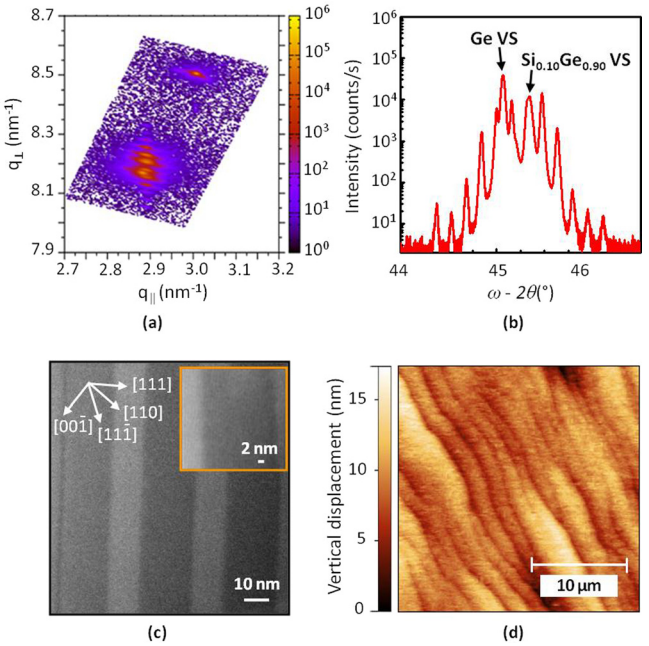

FIG. 2. Structural analysis of sample A: (a) HR-XRD reciprocal space map around the Si (224) Bragg reflection; (b) ω - 2θ scan extracted from symmetric Bragg (333) reflection; the diffraction peaks related to the Ge and $Si_{0.1}Ge_{0.9}$ layers in the VS are indicated by arrows; (c) high-angle annular dark field STEM cross section image of Ge QWs; the inset shows a high magnification image of the same QW structure; (d) AFM image of the top surface.

Table II. Samples A and B are characterized by a comparable coherence and sharpness of QW interfaces, as indicated by the fact that the HR-XRD ω-2θ scan and TEM images obtained in the two cases are very similar. On the other hand, a significantly higher TDD of $(2.5 \pm 0.9) \times 10^8\,\mathrm{cm}^{-2}$ is found in the case of sample B, as expected. Finally, a surface morphology similar to that of sample A is observed in the case of sample B, even though a RMS surface roughness of only (1.1 ± 0.1) nm has been measured through AFM scans on $5 \times 5\,\mu\mathrm{m}^2$ areas for sample B. The comparison between samples A and B suggests that the insertion of the annealed Ge layer leads to an increased surface roughness. As mentioned before, the structural properties of sample C can be used as a high-quality benchmark. The XRD analysis suggests that in sample A the same interface quality of sample C has been reached. On the other hand, the TDD is about one order of magnitude higher for substrate A with respect to substrate C, in which the grading yields a low TDD of $(3 \pm 1) \times 10^6\,\mathrm{cm}^{-2}$. Finally, a similar surface roughness RMS value of (2.3 ± 0.3) nm has been found for sample C on the same scanning area. Sample C is characterized by a cross-hatch pattern typical of graded buffers (Ref. 32). This comparison indicates that the structural quality of sample A is close to that of sample C, but for the higher TDD.

TABLE II. TDD and surface roughness of the studied samples.

Sample	TDD	Surface roughness
A	$(2.7 \pm 0.6) \times 10^7\,\mathrm{cm}^{-2}$	2.1 ± 0.3 nm
B	$(2.5 \pm 0.9) \times 10^8\,\mathrm{cm}^{-2}$	1.1 ± 0.1 nm
C	$(3 \pm 1) \times 10^6\,\mathrm{cm}^{-2}$	2.3 ± 0.3 nm

IV. BAND STRUCTURE OF Ge/SiGe QWs ON Si(111)

The effects of the confinement in the [111] direction and of the biaxial strain applied in the (111) plane have been evaluated through the calculation of the band structure of Ge/SiGe QWs on Si(111). The actual thickness, composition and strain values of the QW stack of sample A, as obtained from XRD analysis, have been used as input parameters for the calculation. Band alignment and confined states have been calculated, using the set of deformation potentials reported in Ref. 34 and the Nextnano software package.[35] Eight-band k·p has been used to obtain the energy levels and the envelope functions for heavy-holes, light-holes, split-off and electron states at the Γ point of the Brillouin zone. The envelope functions and energy levels of electrons at L and Δ valleys have been calculated within the effective mass approximation.[36] The band alignment and the square modulus of the wavefunction of the first confined level of each band are reported in Fig. 3.

A type-I band alignment is obtained for the direct band gap. There is a character inversion between the top of the valence band in well and barrier regions, due to the different nature of the strain (tensile in the barriers and compressive in the well). This difference results into a higher offset for HH states. These features are commonly observed also in Ge/SiGe QWs on Si(001).[2] On the contrary, L-type states are

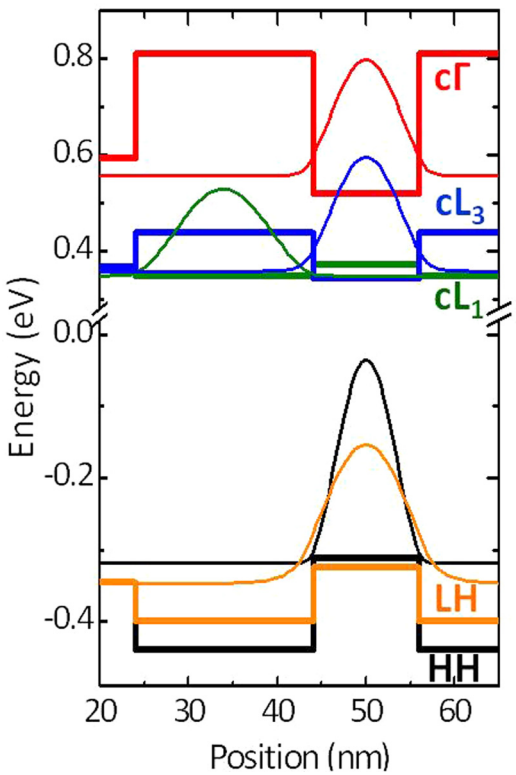

FIG. 3. Band alignment of strain-compensated $Ge/Si_{0.15}Ge_{0.85}$ QWs grown on the (111) plane. The square modulus of the wavefunction of the first confined level is also shown for each band. Note the type-II band alignment of the cL_1 band. The calculation, performed with the structural parameters of sample A, refers to RT.

split due to the compressive strain in the (111) plane that breaks the degeneracy of L valleys giving rise to two groups of states constituted by the minimum in the [111] direction ("cL_1") and by the three degenerate minima in the [−111], [1−11], [11−1] directions ("cL_3"), respectively.[17,37] As shown in Fig. 3, in Ge QWs the compressive strain causes cL_3-type states to be the lowest conduction states. While a type-I band alignment is still predicted for cL_3 levels, cL_1 states are characterized by a type-II band alignment, with electrons confined in the barrier region. Consequently, cL_1 confined states are not expected to contribute significantly to the optical behavior of the system.

V. OPTICAL PROPERTIES OF Ge/SiGe QWs ON Si (111)

The RT ABS spectrum of sample A is reported in Fig. 4(b). The staircase shape typical of direct transitions between Γ-type confined states in Ge/SiGe QWs[29] is clearly observed. In Fig. 4(a), the band alignment calculated for sample A (see Sec. IV) is reported, together with the confined levels involved in the low energy transitions. In Fig. 4(b) the transition energies, given by the calculation, are reported as arrows. The comparison allows the attribution of the experimental features at about 0.88 eV, 0.90 eV, and 0.97 eV to the direct HH1-cΓ1, LH1-cΓ1, and HH2-cΓ2 transitions, respectively. A good agreement between experimental and calculated transition energies is found. As commonly observed in Ge QWs on Si(001),[2] no features unambiguously related to indirect transitions involving confined conduction band states at L can be observed due to the limited number of periods. The spectrum of sample A is characterized by the lack of excitonic peaks, unlike sample C (see the inset of Fig. 4(b)). This can be related to the higher TDD. Indeed, TDs contribute to reduce the excitonic resonances because (i) they enhance the exciton scattering, and (ii) induce local QW thickness fluctuations[33] with an ensuing broadening of the exciton resonances.

The RT PL spectrum of sample A is reported in Fig. 5 (black full line). The emission band at 0.85 eV can be associated to the cΓ1-HH1 direct recombination, as indicated by the comparison with the ABS spectrum reported in Fig. 4(b). Taking into account the energies of the confined levels reported in Fig. 4(a), the broad band centered at about 0.7 eV is attributed to the indirect $cL_3$1-HH1 recombination. Due to thermal broadening effects, the zero-phonon line and the different phonon replica cannot be resolved at RT. No features related to the $cL_1$1-HH1 recombination are observed due to the type-II band alignment and to the superposition with the $cL_3$1-HH1 emission band. The feature centered at about 0.77 eV can be attributed to the direct recombination in the slightly tensile-strained Ge layer of the VS. Indeed, the RT PL spectrum of substrate A (not shown) is characterized by the presence of the same emission band.

In Fig. 5, the PL spectra of samples B and C (green dotted line and red dash-dotted line, respectively), measured under identical experimental conditions as the PL of sample A, are also shown. The PL spectrum of sample B is similar to that of sample A. No features are visible at 0.77 eV, as

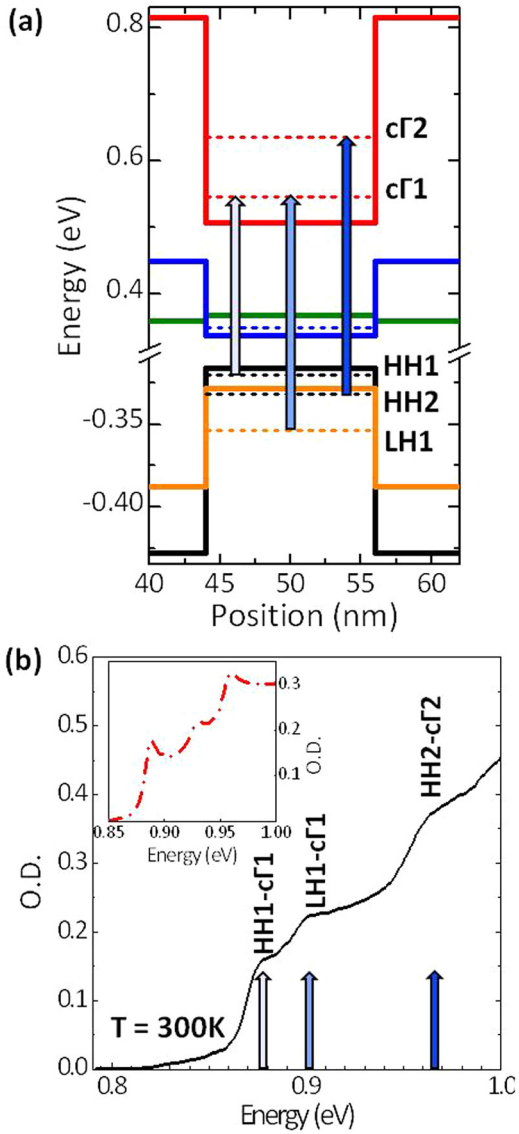

FIG. 4. (a) Lower energy confined levels (dashed lines) of the conduction and valence band of sample A. The direct transitions observed in ABS spectra are also shown as arrows. (b) RT ABS spectrum of sample A. The calculated energies of the HH1-cΓ1, LH1-cΓ1, and HH2-cΓ2 transitions are indicated by the arrows. In the inset, the RT ABS spectrum of sample C is also reported for reference.

expected due to the absence of a Ge layer in the VS of this sample. The overall emitted intensity in sample A is about one order of magnitude higher than that in sample B, which can be explained in terms of a significantly lower TDD in sample A (see Table II). This evidence further confirms that the annealed Ge layer reduces the TDD in the VS, as shown by defect etching measurements, and this reduction is maintained also in the QW stack.

The shape and the transition energies observed in the PL spectrum of sample A are similar to that of sample C, despite the different substrate orientation. However, the integrated intensity emitted by sample A is more than one order of magnitude lower than that of sample C, indicating that a further optimization is still required in order to fully reproduce the structural and optical quality of the benchmark structure.

Figure 6 displays the PL spectrum of sample A measured at T = 5 K. In analogy to the case of Ge QWs on Si

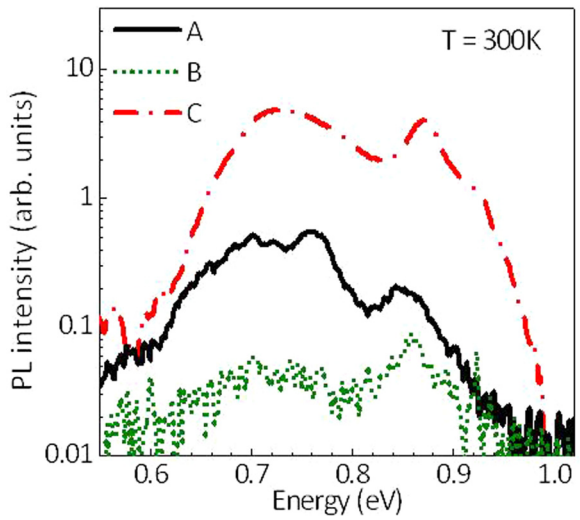

FIG. 5. RT PL spectra of sample A (black full line), B (green dotted line), and C (red dash-dotted line). Note the logarithmic scale of the vertical axis.

(001) (see the inset), the low temperature PL spectrum is dominated by the indirect emission.[38] Taking into account the attribution of the structures of the RT PL spectrum and the expected band gap shrinkage, the feature at 0.94 eV is attributed to the direct cΓ1-HH1 emission.[15] The weak band at higher energies can be due to the cΓ2-HH2 recombination in analogy to the case of Ge QWs on Si(001). The peaks visible at about 0.73 and 0.76 eV can be associated to the zero-phonon line and the LA replica of the indirect cL_31-HH1 transition. Again, no features clearly due to the cL_11-HH1 recombination can be observed. As a matter of fact, due to the type-II band alignment and to the lower density of states with respect to the cL_3 minima, the cL_11-HH1 emission is expected to be very weak. Moreover, because of the small energy distance of the cL_31 levels from the cL_11 levels (of the order of 10 meV in sample A), the cL_11-HH1 emission band could be eventually hidden by the much more intense cL_31-HH1 one.

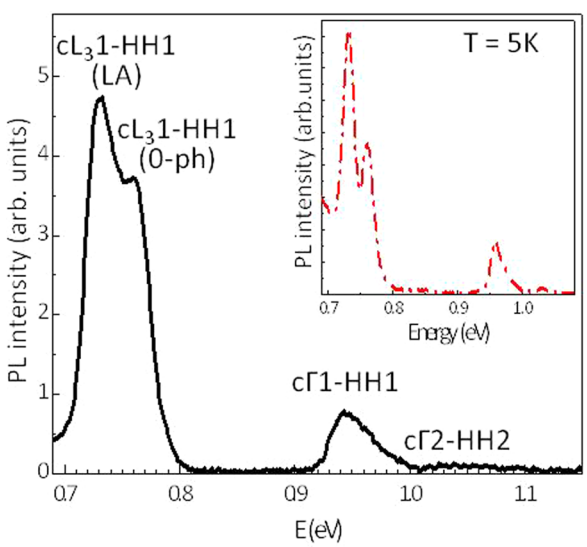

FIG. 6. PL spectrum of sample A at T = 5 K. In the inset, the PL spectrum of sample C at T = 5 K is reported as a reference.

VI. CONCLUSIONS

The epitaxial growth of $Ge/Si_{0.15}Ge_{0.85}$ QWs on Si(111) via LEPECVD has been demonstrated. A 3 μm thick double step buffer approach has been used for the deposition. This VS allows to circumvent the limits typical for the growth on Si(111) and features a TDD of only one order of magnitude higher than that characterizing Ge-rich heterostructures grown on Si(001) through a much thicker GVS. The ABS and emission properties of $Ge/Si_{0.15}Ge_{0.85}$ QWs on Si(111) have been studied; the observed transition energies are in good agreement with theoretical predictions. Furthermore, the optical spectra of the active part of the structure are comparable to those of high quality Ge/SiGe QWs grown on Si(001) through thick GVSs, both in terms of PL intensity and of shape of the ABS and PL spectra.

In conclusion, with the presented approach, that can be extended to other Ge-rich heterostructures, we propose a viable path towards the integration of high quality Ge/SiGe QWs on Si(111). Further improvements of the structural and optical properties may eventually be achieved through an optimization of the VS design and through a proper tailoring of growth parameters. The possibility to integrate Ge-rich layers on the (111) surface may open up alternative ways towards the development of Ge-based systems with novel optical properties and towards the control of the dislocation dynamics.

ACKNOWLEDGMENTS

The authors acknowledge the financial support provided by Fondazione Cariplo through the DefCon4 Project (Grant 2011-0331) and EIDOS project (Grant 2011-0382), by Regione Lombardia through the grant Dote Ricercatori and by the EC ICT FET Proactive Initiative Towards Zeropower ICT through the GREEN Silicon Project (No. 257750). Professor M. Guzzi is gratefully acknowledged for fruitful discussions.

[1]Y. H. Kuo, Y. K. Lee, Y. Ge, S. Ren, J. E. Roth, T. I. Kamins, D. A. B. Miller, and J. S. Harris, Nature **437**, 1334 (2005).
[2]M. Bonfanti, E. Grilli, M. Guzzi, M. Virgilio, G. Grosso, D. Chrastina, G. Isella, H. von Känel, and A. Neels, Phys. Rev. B **78**, 041407 (2008).
[3]C. Lange, N. S. Köster, S. Chatterjee, H. Sigg, D. Chrastina, G. Isella, H. von Känel, M. Schäfer, M. Kira, and S. W. Koch, Phys. Rev. B **79**, 201306 (2009).
[4]Y. Busby, M. De Seta, G. Capellini, F. Evangelisti, M. Ortolani, M. Virgilio, G. Grosso, G. Pizzi, P. Calvani, S. Lupi, M. Nardone, G. Nicotra, and C. Spinella, Phys. Rev. B **82**, 205317 (2010).
[5]S. A. Claussen, E. Tasyurek, J. E. Roth, and D. A. B. Miller, Opt. Express **18**, 25596 (2010).
[6]F. Pezzoli, F. Bottegoni, D. Trivedi, F. Ciccacci, A. Giorgioni, P. Li, S. Cecchi, E. Grilli, Y. Song, M. Guzzi, H. Dery, and G. Isella, Phys. Rev. Lett. **108**, 156603 (2012).
[7]P. Chaisakul, D. Marris-Morini, J. Frigerio, D. Chrastina, M.-S. Rouifed, S. Cecchi, P. Crozat, G. Isella, and L. Vivien, Nat. Photonics **8**, 482 (2014).
[8]A. Giorgioni, F. Pezzoli, E. Gatti, S. Cecchi, C. Kazuo Inoki, C. Deneke, E. Grilli, G. Isella, and M. Guzzi, Appl. Phys. Lett. **102**, 012408 (2013).
[9]P. Chaisakul, D. Marris-Morini, G. Isella, D. Chrastina, N. Izard, X. Le Roux, S. Edmond, J. Coudevylle, and L. Vivien, Appl. Phys. Lett. **99**, 141106 (2011).
[10]K. Gallacher, P. Velha, D. J. Paul, S. Cecchi, J. Frigerio, D. Chrastina, and G. Isella, Appl. Phys. Lett. **101**, 211101 (2012).

[11]A. Samarelli, L. Ferre Llin, S. Cecchi, J. Frigerio, T. Etzelstorfer, E. Müller, Y. Zhang, J. R. Watling, D. Chrastina, G. Isella, J. Stangl, J. P. Hague, J. M. R. Weaver, P. Dobson, and D. J. Pau, J. Appl. Phys. **113**, 233704 (2013).
[12]E. A. Fitzgerald, Y.-H. Xie, M. L. Green, D. Brasen, A. R. Kortan, J. Michel, Y.-J. Mii, and B. E. Weir, Appl. Phys. Lett. **59**, 811 (1991).
[13]C. Rosenblad, H. von Känel, M. Kummer, A. Dommann, and E. Müller, Appl. Phys. Lett. **76**, 427 (2000).
[14]S. Marchionna, A. Virtuani, M. Acciarri, G. Isella, and H. von Känel, Mater. Sci. Semicond. Process. **9**, 802 (2006).
[15]E. Gatti, E. Grilli, M. Guzzi, D. Chrastina, G. Isella, and H. von Känel, Appl. Phys. Lett. **98**, 031106 (2011).
[16]S. Cecchi, E. Gatti, D. Chrastina, J. Frigerio, E. Müller Gubler, D. J. Paul, M. Guzzi, and G. Isella, J. Appl. Phys. **115**, 093502 (2014).
[17]H. S. Lan, S.-T. Chan, T.-H. Cheng, C.-Y. Chen, S.-R. Jan, and C. W. Liu, Appl. Phys. Lett. **98**, 101106 (2011).
[18]J. M. Tang, B. T. Collins, and M. E. Flatté, Phys. Rev. B **85**, 045202 (2012).
[19]Y. J. Yang, W. S. Ho1, C.-F. Huang, S. T. Chang, and C. W. Liu, Appl. Phys. Lett. **91**, 102103 (2007).
[20]A. Zhylik, A. Benediktovich, A. Ulyanenkov, H. Guerault, M. Myronov, A. Dobbie, and D. R. Leadley, J. Appl. Phys. **109**, 123714 (2011).
[21]J. Parsons, E. H. C. Parker, D. R. Leadley, T. J. Grasby, R. J. H. Morris, and A. Capewell, Appl. Phys. Lett. **91**, 063127 (2007).
[22]T. S. Kuan and S. S. Iyer, Appl. Phys. Lett. **59**, 2242 (1991).
[23]M. L. Lee, D. A. Antoniadis, and E. A. Fitzgerald, Thin Solid Films **508**, 136 (2006).
[24]V. Destefanis, J. M. Hartmann, A. Abbadie, A. M. Papon, and T. Billon, J. Cryst. Growth **311**, 1070 (2009).
[25]A. Dobbie, V. H. Nguyen, M. Myronov, T. E. Whall, E. H. C. Parker, and D. R. Leadley, Appl. Phys. Express **5**, 071301 (2012).
[26]V. Huy Nguyen, A. Dobbie, M. Myronov, D. J. Norris, T. Walther, and D. R. Leadley, Thin Solid Films **520**, 3222 (2012).
[27]T. F. Wietler, A. Ott, E. Bugiel, and K. R. Hofmann, Mater. Sci. Semicond. Process. **8**, 73 (2005).
[28]H. Luan, D. R. Lim, K. K. Lee, K. M. Chen, J. G. Sandland, K. Wada, and L. C. Kimerling, Appl. Phys. Lett. **75**, 2909 (1999).
[29]M. Bonfanti, E. Grilli, M. Guzzi, D. Chrastina, G. Isella, H. von Känel, and H. Sigg, Physica E **41**, 972 (2009).
[30]V. A. Shah, A. Dobbie, M. Myronov, D. J. F. Fulgoni, L. J. Nash, and D. R. Leadley, Appl. Phys. Lett. **93**, 192103 (2008).
[31]Y. Yamamoto, G. Kozlowski, P. Zaumseil, and B. Tillack, Thin Solid Films **520**, 3216 (2012).
[32]D. Chrastina, B. Rössner, G. Isella, H. von Känel, J. P. Hague, T. Hackbarth, H.-J. Herzog, K.-H. Hieber, and U. König. *LEPECVD—A Production Technique for SiGe MOSFETs and MODFETs, in Materials for Information Technology*, edited by E. Zschech, C. Whelan, and T. Mikolajick, (Springer, 2005), pp. 17–29.
[33]S. Cecchi, T. Etzelstorfer, E. Müller, A. Samarelli, L. Ferre Llin, D. Chrastina, G. Isella, J. Stangl, J. M. R. Weaver, P. Dobson, and D. J. Paul, J. Electron. Mater. **42**, 2030 (2013).
[34]D. J. Paul, Phys. Rev. B **77**, 155323 (2008).
[35]S. Birner, T. Zibold, T. Andlauer, T. Kubis, M. Sabathil, A. Trellakis, and P. Vogl, IEEE Trans. Electron. Dev. **54**, 2137 (2007).
[36]J. H. Davies, *The Physics of Low-dimensional Semiconductors* (Cambridge University Press, 1997).
[37]D. Rideau, M. Feraille, L. Ciampolini, M. Minondo, C. Tavernier, and H. Jaouen, Phys. Rev. B **74**, 195208 (2006).
[38]The PL spectrum of sample A reflects the general behavior of Ge/SiGe QWs grown on Si(001) through GVSs[15] in terms of band shape, relative intensity of the different structures and temperature dependence (not shown). In the same work, the transition energies of Ge/SiGe QWs have been demonstrated to follow the Varshni law of bulk Ge (see, e.g., the inset of Fig. 2). The emission band at 0.77 eV due to the direct recombination of the Ge layer of the VS, visible in the RT PL spectrum of sample A, is present also at LT, but it cannot be resolved from the indirect emission band of the Ge QWs, as demonstrated by the temperature evolution of the spectrum (not shown).